Electronic Supplementary Information for

Understanding the effect of the co-sensitizing ratio on the surface potential, electron injection efficiency, and Förster resonance energy transfer

Jie Yang[a], Xing-Liang Peng[b], Zhu-Zhu Sun[c], Shuai Feng[d], Wei-Lu Ding[e], Hong-Yan He[e], and Ze-Sheng Li*[a]*

a Beijing Key Laboratory of Photoelectronic/Electrophotonic Conversion Materials, Key Laboratory of Cluster Science of Ministry of Education, School of Chemistry, Beijing Key Laboratory for Chemical Power Source and Green Catalysis, School of Chemistry, Beijing Institute of Technology, Beijing 100081, China
b MOE Key Laboratory of Organic OptoElectronics and Molecular Engineering, Department of Chemistry, Tsinghua University, Beijing 100084, People's Republic of China
c Energy-Saving Building Materials Innovative Collaboration Center of Henan Province, Xinyang Normal University, Xinyang, 464000, China
d College of Chemistry and Chemical Engineering, Taishan University, Taian, 271021, China
e Beijing Key Laboratory of Ionic Liquids Clean Process, CAS Key Laboratory of Green Process and Engineering, State Key Laboratory of Multiphase Complex Systems, Institute of Process Engineering, Chinese Academy of Sciences, Beijing 100190, China

Corresponding Author

* Wei-Lu Ding (wlding@ipe.ac.cn)

* Ze-Sheng Li (zeshengli@bit.edu.cn)

Contents

Orientation factor..……...……...……..…….. ……..S3

Newns−Anderson model..……...……...……..…….. ……S4

Reorganization energy..……...……...……..…….. ……...S5

Fig. S1. The different configurations in Model **1** …… S6

Fig. S2. The different configurations in Model **2**……..S7

Fig. S3. The tilt angle between the axes of the dipole moment and the surface normal of the TiO_2 film……... S8

Fig. S4. The unoccupied molecular orbitals of whole adsorbents of Model **1** and **2**……..…..S9

Fig. S5. The excitation energies of IQ21 and emission energies of S2 *vs*. simulated time span……..S10

Fig. S6. Co-sensitizing models on grid of Ti atoms for Model **3** and **4**……..S11

Fig. S7. The different configurations in Model **3**……S12

Fig. S8. The different configurations in Model **4**……S13

Fig. S9. Orientation factor and donor-acceptor distance..……...……...……..S14

Fig. S10. The scaled FRET rate of varied D-A couples……..……..……..S15

Table S1. The vertical excited state/wavelength tested by different functionals.……...S16

Table S2. The distances between the O of carboxyl of adsorbent and Ti on the surface….....S17

Table S3 Adsorption density and adsorption energy in Models **3** and **4**…….....…….S18

Table S4 The surface dipole concentration and surface potential change in Models **3** and **4**…S19

Table S5 Electron injection, electron-hole recombination, electron injection efficiency in Models **3** and **4**..…….....S20

Table S6 FRET geometrical parameters in Models **3** and **4**..…….S21

Theoretical background

1 Orientation factor

The orientation factor κ^2 is expressed by the followed equation:[1-3]

$$\kappa^2 = (\sin\alpha_D \sin\alpha_A \cos\beta_{DA} - 2\cos\alpha_D \cos\alpha_A)^2 \quad (1)$$

$$\alpha_D = \arccos(\sin\theta_D \sin\phi_D) \quad (2)$$

$$\alpha_A = \arccos(\sin\theta_A \sin\phi_A)$$

$$\beta_{DA} = \arctan(\tan\theta_D \cos\phi_D) - \arctan(\tan\theta_A \cos\phi_A)$$

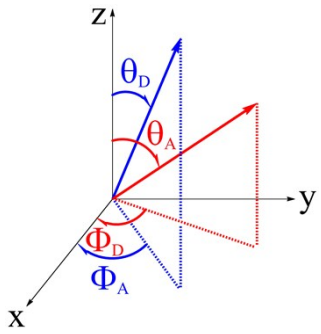

Scheme S1. Angles θ and Φ define the relative orientation of D-A couple.

where the angles θ and Φ define the relative orientation between the two interacting dipole moments. Notably, the κ^2 can vary from 0 to 4 (κ^2 = 0, 1, 4 upon the transition dipole moment of energy donor and acceptor is vertical, parallel, and end to end, respectively, and κ^2 = 2/3 of the random orientation).

2 Newns−Anderson model[4]

To obtain a relatively accurate electron-transfer time, Newns−Anderson approach was employed to compute the mixing of lowest unoccupied molecular orbital (LUMO) on sensitizer with the manifold virtue orbitals on TiO_2. Accordingly, this mixing possesses a Lorentzian distribution:

$$\rho_{\mathrm{LUMO}}(E) = \frac{1}{(E - E_{\mathrm{LUMO}}(\mathrm{ads}))^2 + (\frac{\hbar\Gamma}{2})^2} \qquad (3)$$

The broadening width $\hbar\Gamma$ in Eq (3) is taken as the mean deviation of the LUMO (sensitizer) levels, and is defined as follows:

$$\hbar\Gamma = \sum_i p_i \left| \varepsilon_i - E_{\mathrm{LUMO}}(\mathrm{ads}) \right| \qquad (4)$$

where $E_{\mathrm{LUMO}}(\mathrm{ads})$ is obtained by a weighted average:

$$E_{\mathrm{LUMO}}(\mathrm{ads}) = \sum_i p_i \varepsilon_i \qquad (5)$$

where P_{i} and ε_i are the portion of ith molecular orbital (MO) for sensitizer and its corresponding MO energy, respectively. Simultaneously, the P_{i} is evaluated by:

$$P_i = \frac{\sum_{j}^{A \in \mathrm{sen}} (c_{ij}^{A})^2}{\sum_{j}^{A \in \mathrm{sen@TiO_2}} (c_{ij}^{A})^2} \qquad (6)$$

3 Reorganization energy[5]

For the χ is the inner reorganization energy which contains the solute part χ^{sen} and the solvent part χ^{sol}

$$\chi = \frac{\chi_1^{sen} + \chi_2^{sen}}{2} \tag{7}$$

Accordingly, the χ^{sen} can be defined as:

$$\chi_1^{sen} = E_{(Q_P)}^{DBA^*} - E_{(Q_r)}^{DBA^*} \tag{8}$$

$$\chi_2^{sen} = E_{(Q_r)}^{DBA^+} - E_{(Q_P)}^{DBA^+} \tag{9}$$

where the $E_{(Q_P)}^{DBA^*}$, $E_{(Q_r)}^{DBA^*}$, $E_{(Q_r)}^{DBA^+}$ and $E_{(Q_P)}^{DBA^+}$ contribute to the energies obtained from the excited state at the form of cation, energies of the relaxed excited state, the cationic energies calculated at the geometry of the excited state and the energies of the relaxed cationic state, respectively.

As for the content related to χ^{sol}, it is expressed by:

$$\chi^{sol} = \Delta q\left(\frac{1}{2R_D} + \frac{1}{2R_A} - \frac{1}{R}\right)\left(\frac{1}{\varepsilon_\infty} - \frac{1}{\varepsilon_s}\right) \tag{10}$$

where R_D, R_A, R denote the radii of the donor, acceptor and the distances between their centers, and the ε_∞ as well as the ε_s stand for the optical frequency and static relative dielectric constants of the solvent, respectively. And Δq is the amount of the transferred electron.

Figures

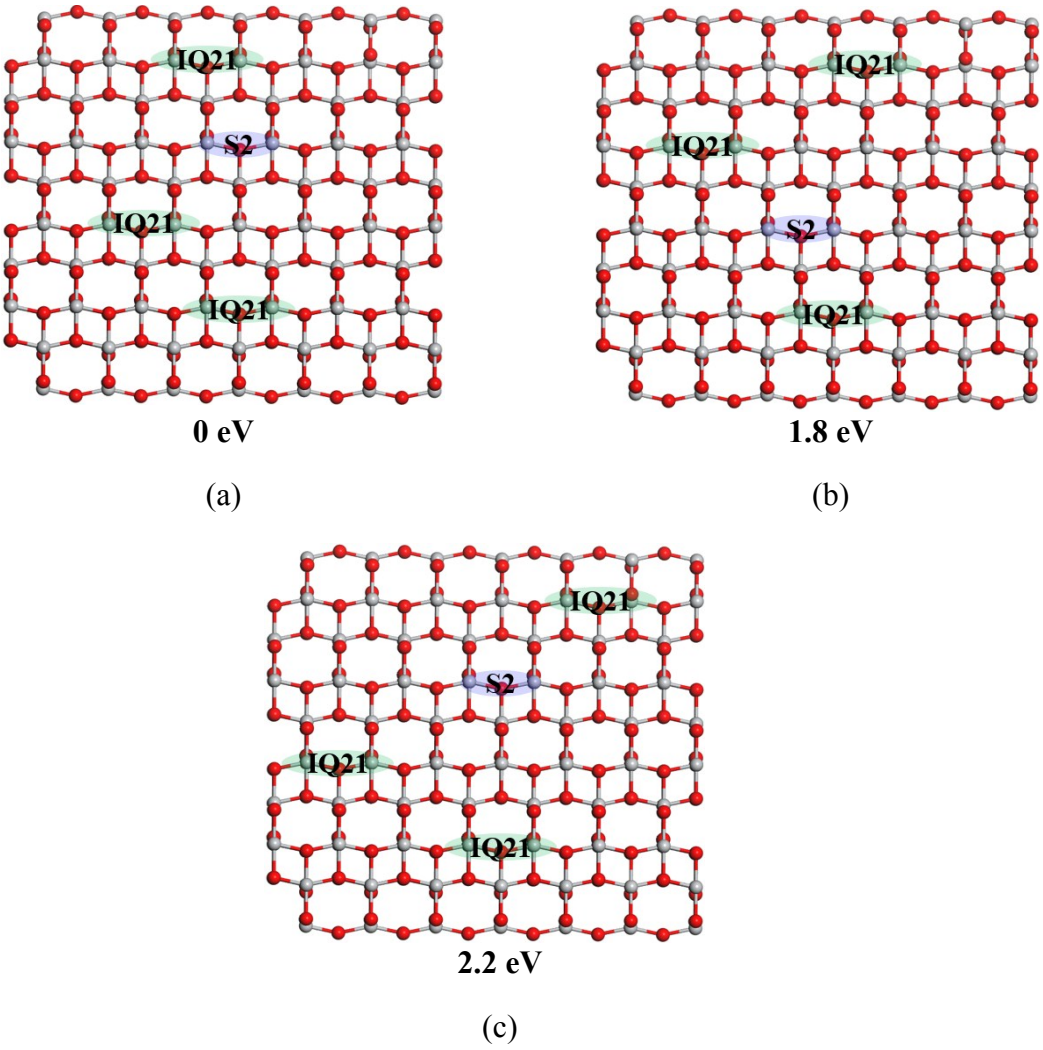

Model **1**

Fig. S1. (a)-(c) The different configurations in Model **1** (the energy labelled in each configuration represents for the relative energy, and the green as well as purple present for the positions of IQ21 and S2, respectively).

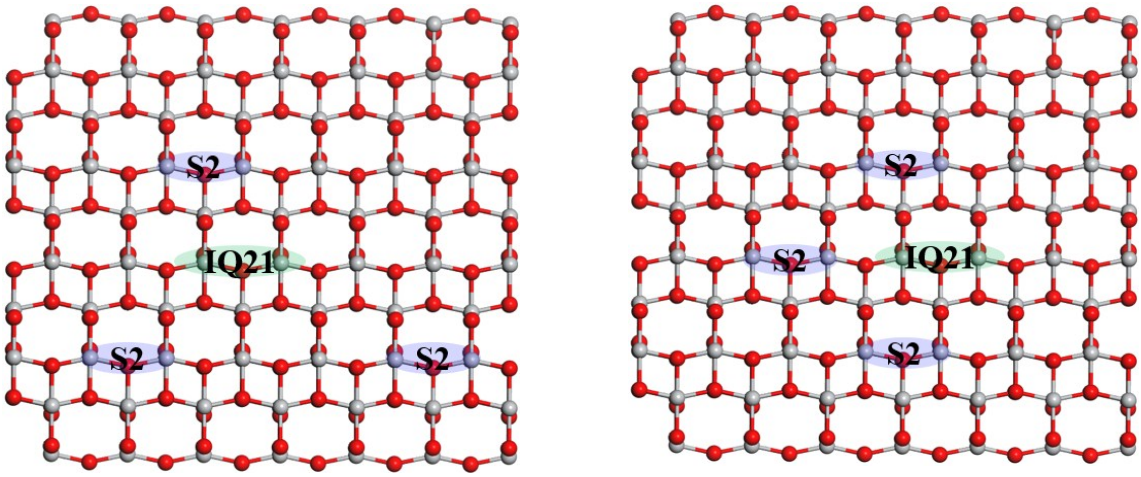

(a) (b)

Model **2**

Fig. S2. (a)-(b) The different configurations in Model **2** (the energy labelled in each configuration represents for the relative energy, and the green as well as purple present for the positions of IQ21 and S2, respectively).

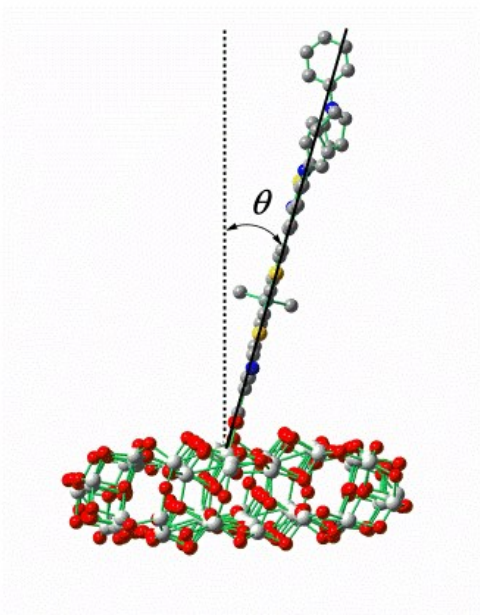

Fig. S3. The tilt angle (θ) between the axes of the dipole moment (μ) and the surface normal of the TiO_2 film.

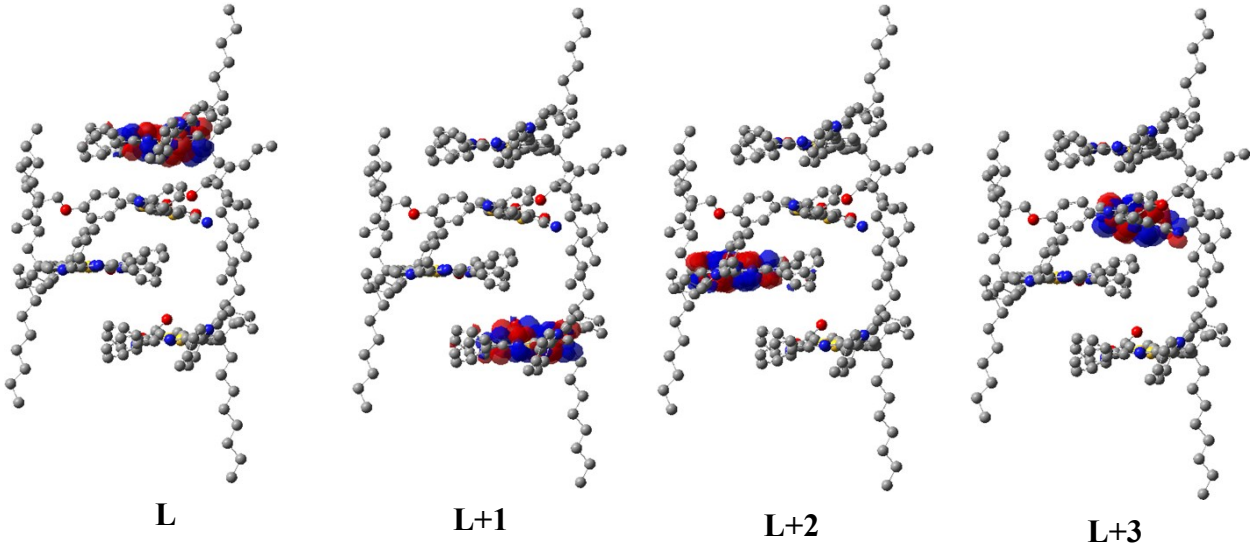

(a) Model **1** (IQ21/S2-3/1)

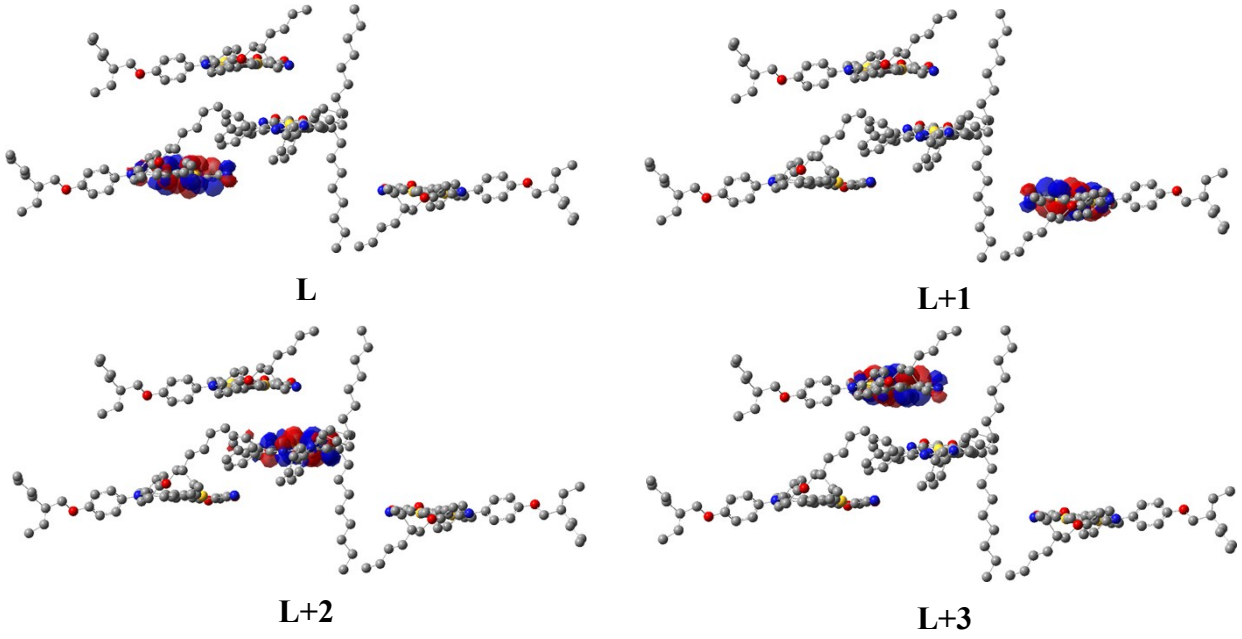

(b) Model **2** (S2/IQ21-3/1)

Fig. S4. The unoccupied molecular orbitals of whole adsorbents in Model **1** and **2**.

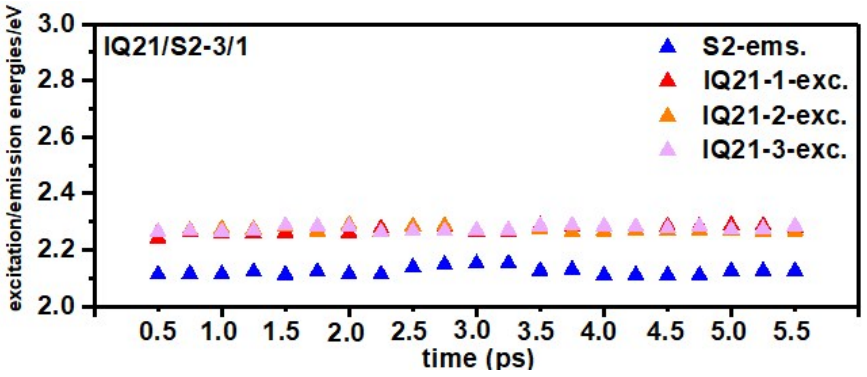

(a)

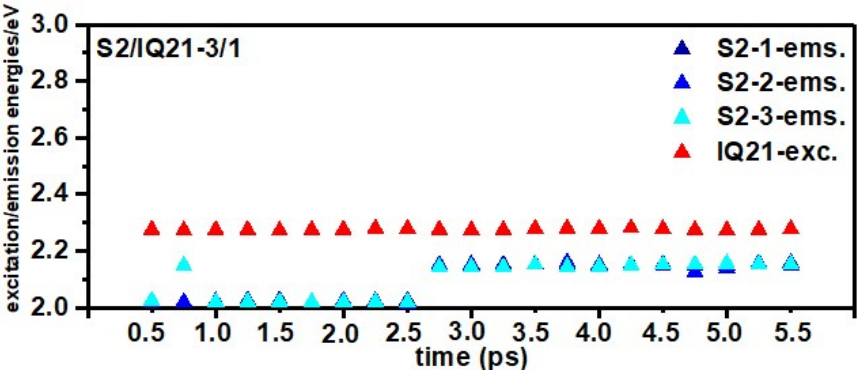

(b)

Fig. S5. The excitation energies of IQ21 and emission energies of S2 *vs*. simulated time span of 5.5 ps: (a) for Model **1** and (b) for Model **2**.

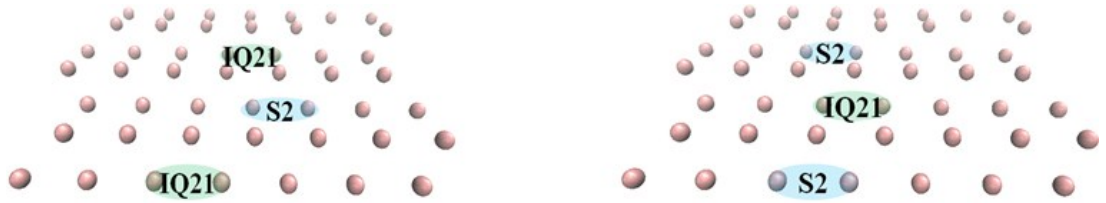

(a) **3** (b) **4**

Fig. S6. Co-sensitizing models on grid of Ti atoms (a) for Model **3** (IQ21/S2-2/1) and (b) for Model **4** (S2/IQ21-2/1).

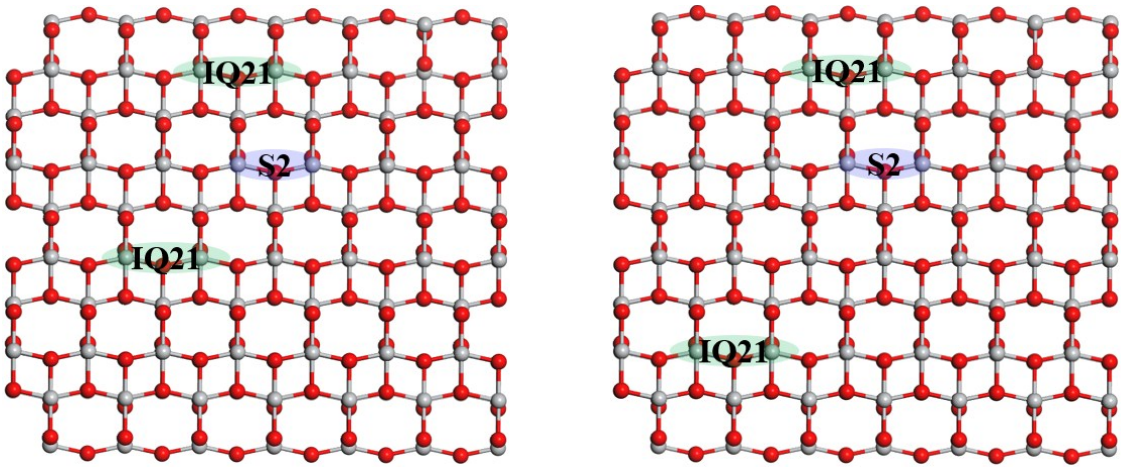

Model **3**

Fig. S7. (a)-(b) The different configurations in Model **3** (the energy labelled in each configuration represents for the relative energy, and the green as well as purple present for the positions of IQ21 and S2, respectively).

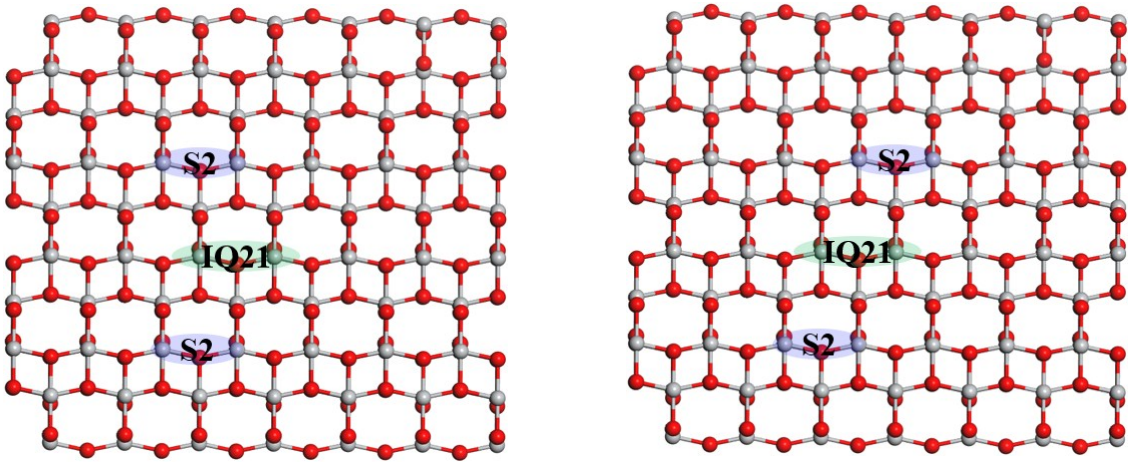

Model **4**

Fig. S8. (a)-(b) The different configurations in Model **4** (the energy labelled in each configuration represents for the relative energy, and the green as well as purple present for the positions of IQ21 and S2, respectively).

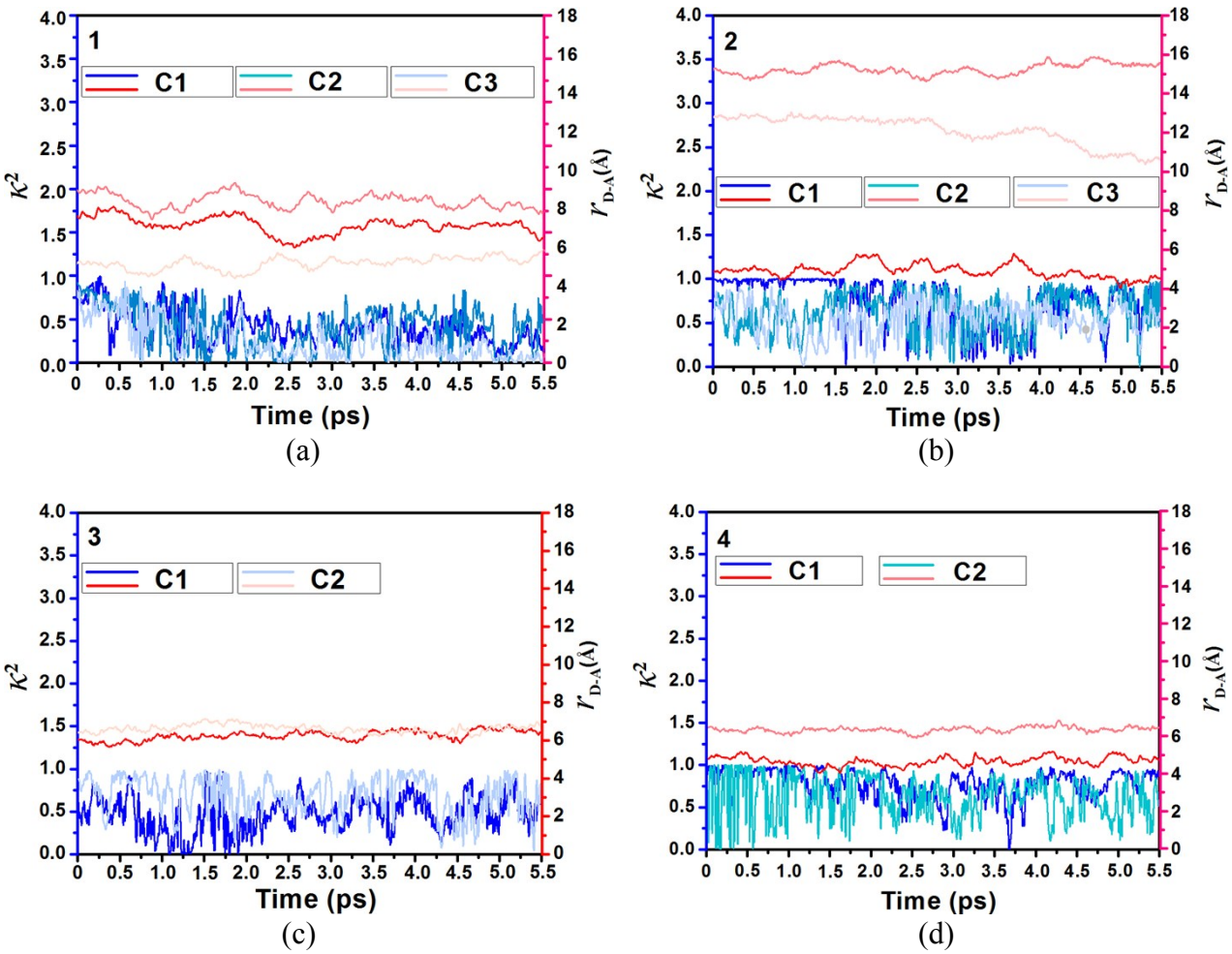

Fig. S9. (a)-(d) Orientation factor κ^2 (the blue series lines) and donor-acceptor distance r_{DA} (the red series lines) as a function of the time span for Models **1**-**4**.

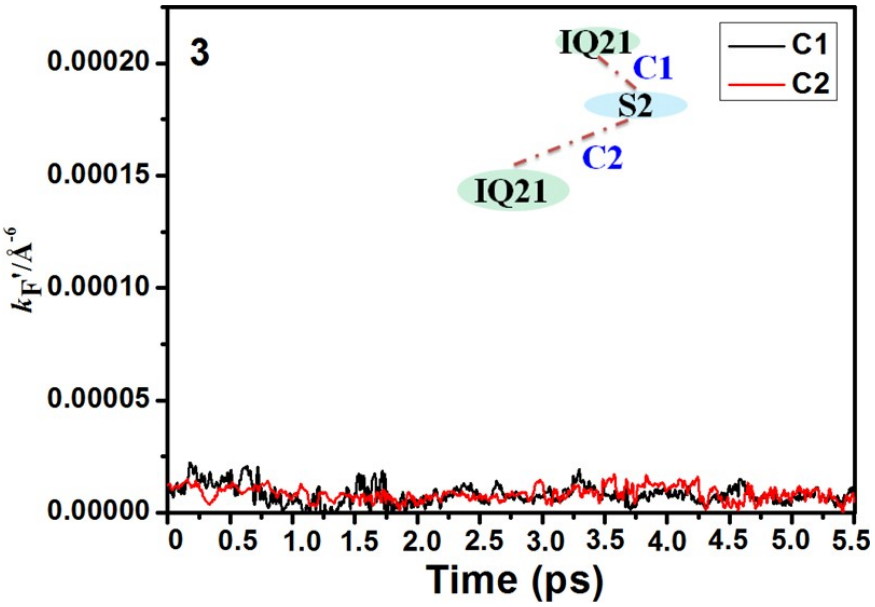

(a)

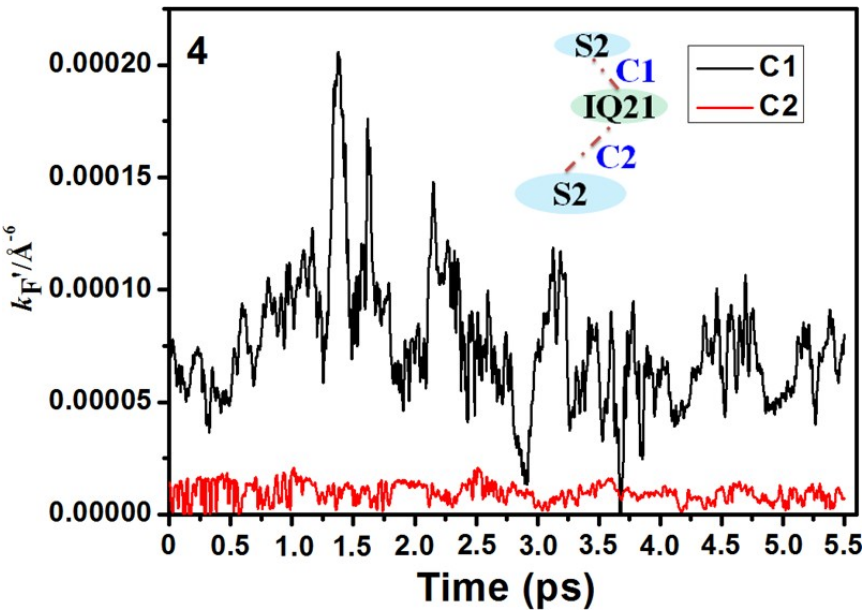

(b)

Fig. S10. The scaled FRET rate k_F' of varied D-A couples (a) for Model **3** and (b) for Model **4** (Cn defines the number of donor-acceptor couple, and the relative alignments between IQ21 and S2 are abstracted from the Fig. S6).

Tables

Table S1. The data (vertical excited state/wavelength) calculated by different functionals of IQ21 and S2 in CH_2Cl_2 solution.

Functionals	B3LYP	CAM-B3LYP	MPW1K	Exp.[a]
IQ21	1.73/715	2.35/528	2.24/553	2.23/557
S2	1.77/699	2.52/492	2.38/522	2.59/478

[a] Experimental values measured in CH_2Cl_2 solution from ref. 40.

Table S2. The distances between the O atom of carboxyl of adsorbent and Ti atom on the surface (unit in Å).

Model	Dye			Co-sensitizer		
	IQ21			S2		
1	2.21/3.50	2.13/2.15	2.14/3.14	2.02/2.90		
2	2.11/2.02			2.02/2.11	2.04/2.11	2.02/2.16

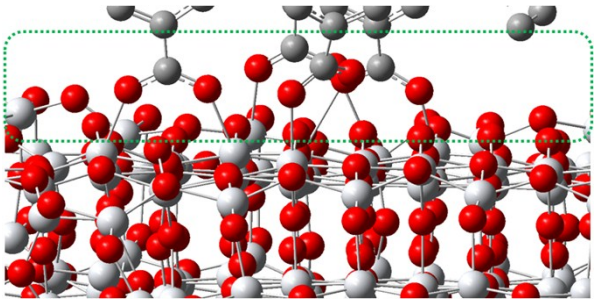

Model **1**

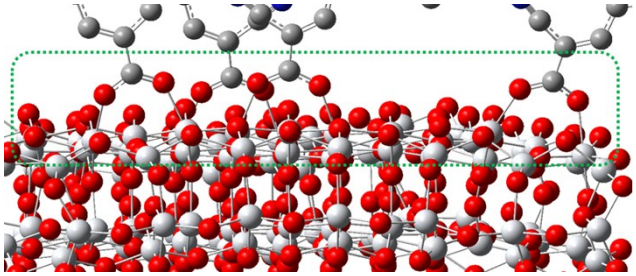

Model **2**

Table S3. Adsorption density ρ(IQ21), ρ(S2), and adsorption energy E_{ads}(IQ21), E_{ads}(S2) in Models **3** and **4**, respectively.

Model	Adsorption density/mol m^{-2}		E_{ads}/eV	
	ρ(IQ21)	ρ(S2)	E_{ads}(IQ21)	E_{ads}(S2)
3	6.08×10^{-7}	3.04×10^{-7}	-5.70, -3.80	-6.89
4	3.04×10^{-7}	6.08×10^{-7}	-8.65	-4.53, -5.21

Table S4. The parameters of surface dipole concentration N_s (unit m^{-2}) and the magnitude of surface potential change ΔV (unit eV) for IQ21 and S2 in Models **3** and **4**.

Model	N_s(IQ21)	N_s(S2)	ΔV(IQ21)	ΔV(S2)
3	0.4×10^{18}	0.2×10^{18}	0.15	0.10
4	0.2×10^{18}	0.4×10^{18}	0.08	0.10

Table S5. Electron injection and electron-hole recombination rate constant, as well as electron injection efficiency in Models **3** and **4**.

Model	k_{inj}/s^{-1} (IQ21)	k_{inj}/s^{-1} (S2)	k_{rec}/s^{-1} (IQ21)	k_{rec}/s^{-1} (S2)	k_{inj}'/s^{-1}	k_{rec}'/s^{-1}	η_{inj}'
3	11.4×10^{15}	18.8×10^{15}	3.1×10^{15}	11.4×10^{15}	67.0×10^{15}	35.4×10^{15}	0.65
	36.8×10^{15}		20.8×10^{15}				
4	34.3×10^{15}	18.6×10^{15}	1.8×10^{15}	4.4×10^{15}	72.4×10^{15}	14.9×10^{15}	0.83
		19.5×10^{15}		8.6×10^{15}			

Table S6. FRET geometrical parameters of κ^2 and r_{DA} and the average k_F' for Models **3** and **4**.

Model	D-A couple(s)	κ^2	r_{DA}/Å	k_F'×10^6(Å^{-6})
3	C1	0.47	6.26	8.11
	C2	0.69	6.61	8.44
4	C1	0.78	4.71	75.28
	C2	0.63	6.35	9.73

References

1. V. Dryza and E. J. Bieske, *J. Phys. Chem. C*, 2014, **118**, 19646-19654.
2. H. Wang, B. Yue, Z. Xie, B. Gao, Y. Xu, L. Liu, H. Sun and Y. Ma, *Phys. Chem. Chem. Phys.*, 2013, **15**, 3527-3534.
3. M. Pastore and F. De Angelis, *J. Phys. Chem. Lett.*, 2012, **3**, 2146-2153.
4. P. Persson, M. J. Lundqvist, R. Ernstorfer, W. A. Goddard and F. Willig, *J. Chem. Theory Comput.*, 2006, **2**, 441-451.
5. J. Preat, *J. Phys. Chem. C*, 2010, **114**, 16716-16725.
6. J. Li, H. Wang, P. Persson and M. Thoss, *J. Chem. Phys.*, 2012, **137**, 22A529.